Design of an Extremely Efficient, Rare-Earth Free, 5 kW Motor in a NEMA 210 Frame

Dorsa Talebi
Dept. of Elec. & Comp. Engr.
Texas A&M University
College Station, TX, USA
dorsa.talebi@tamu.edu

Matthew C Gardner
Dept. of Elec. & Comp. Engr.
University of Texas at Dallas
Richardson, TX, USA
Matthew.Gardner@utdallas.edu

Shrikesh Sheshaprasad
Dept. of Elec. & Comp. Engr.
Texas A&M University
College Station, TX, USA
shrikesh@tamu.edu

Hamid A Toliyat
Dept. of Elec. & Comp. Engr.
Texas A&M University
College Station, TX, USA
toliyat@tamu.edu

Paul Knauer
This Old Part Engineering LLC
San Jose, CA, USA
psknauer@gmail.com

Alan D Crapo
Alan D Crapo Consulting
Sahuarita, AZ, USA
megagauss51@gmail.com

***Abstract*— This paper presents the design of a dual-rotor, conical air gap, axial flux motor with ferrite permanent magnets. This unorthodox topology, which does not use rare earth magnets, enables the design to achieve a much higher efficiency than comparable commercially available NEMA 210 frame motors. Various design aspects, such as winding arrangement and cone angle, are evaluated through 3D finite element analysis, and the selected design has been prototyped and tested. The prototype achieves a peak efficiency above 96.7% and exceeds an efficiency of 96% over a wide range of torques and speeds.**

Keywords—Conical air gap, efficiency, ferrite magnet, grain oriented electrical steel, finite element analysis, permanent magnet synchronous motor, tooth tips

I. INTRODUCTION

This paper presents an unorthodox motor topology design to achieve 5 kW at 1800 RPM in a NEMA 210 frame size, while maintaining an efficiency of over 96% for the US Department of Energy's Next Generation Electric Machines: Enabling Technologies program [1]. Thus, the proposed motor provides an extremely efficient alternative to comparably rated industrial motors. Additionally, this motor employs ferrite permanent magnets (PMs) and does not require rare-earth PMs. Table I provides a list of some comparable NEMA 210 frame motors. Also, the NEMA Premium efficiency for a 4 pole, 5 kW induction motor is only 91.7%, and the corresponding IE4 efficiency is 91.9% [2]. While most NEMA frame motors are induction motors, various other types of motors, including PM motors, synchronous reluctance motors, and switched reluctance motors have been proposed to achieve higher torque densities or efficiencies [2]-[6].

II. MOTOR TOPOLOGY

The proposed motor is a PM motor based on the NovaMAX® motors manufactured by Regal Rexnord®. The topology employs a dual-rotor, single-stator axial flux configuration, as shown in Fig. 1(a). Each rotor has ferrite PMs arranged to concentrate flux into pole pieces made of soft magnetic composite (SMC), as shown in Fig. 1(b). The flux from these pole pieces travels through the conical air gap to the stator. Because the flux in the stator is almost entirely in the axial direction, grain oriented electrical steel (GOES) is used to form the stator teeth. When used in areas with unidirectional flux, GOES can outperform non-oriented electrical steel and improve the machine's torque density and efficiency [10]-[14]. The windings are wrapped around the stator teeth, as shown in Fig. 1(c).

TABLE I. NEMA 210 FRAME MOTORS

Motor Type	Rated Speed (RPM)	Rated Torque (Nm)	Rated Power (kW)	Nominal Efficiency (%)	Reference
Induction	1800	39.6	7.5	92.1	[7]
PM	1800	39.6	7.5	94.5	[7]
Synchronous Reluctance	1800	29.5	5.9	90.2	[8]
PM-assisted Synchronous Reluctance	1800	41.4	7.8	93.1	[8]
Switched Reluctance	1500	47.4	7.4	86.7	[9]

This topology has already demonstrated the potential for very high efficiency [15]. However, a few changes have been made to the existing motor's topology whose performance was described by [15]. First, instead of wrapping the windings around bobbins that would then be placed over the stator teeth, only a thin layer of insulation was placed between the windings and the stator teeth to facilitate a higher copper fill factor. Second, the air gap surface area was increased by adding a flat section to the stator teeth to match the flat section on the SMC rotor poles, as shown in Fig. 2. (It is impractical to form a sharp angle in the SMC pole pieces, instead.) This paper presents the

This work was supported by the US Department of Energy under award number DE-EE0007875

design of a motor that demonstrates that this topology can produce industrial motors with extremely high efficiencies. A prototype has been built and tested. The experimental testing proves that the topology is capable of obtaining over 96% efficiency, which makes it a great candidate not only for this rating but also for a variety of applications that require an extremely efficient motor design, such as fully or hybrid electrified transportation [16]. However, it should be noted that, although the design has low losses, it has not been optimized to reduce mass. If optimizing mass was critical, the rotor could be replaced with a Halbach array of NdFeB magnets to obtain a high torque density with high efficiency [17]-[20].

III. Motor Design

The impacts of various design decisions including the winding configuration, the cone angle, and the presence or absence of SMC tooth tips, were evaluated using 3D finite element analysis (FEA). ANSYS Maxwell, a commercial FEA package, was used to determine each design's torque, rotor core losses, stator core losses, and stator housing eddy current losses. The bearing losses and stator copper losses were calculated directly. The loss models are explained in more detail and validated in [15].

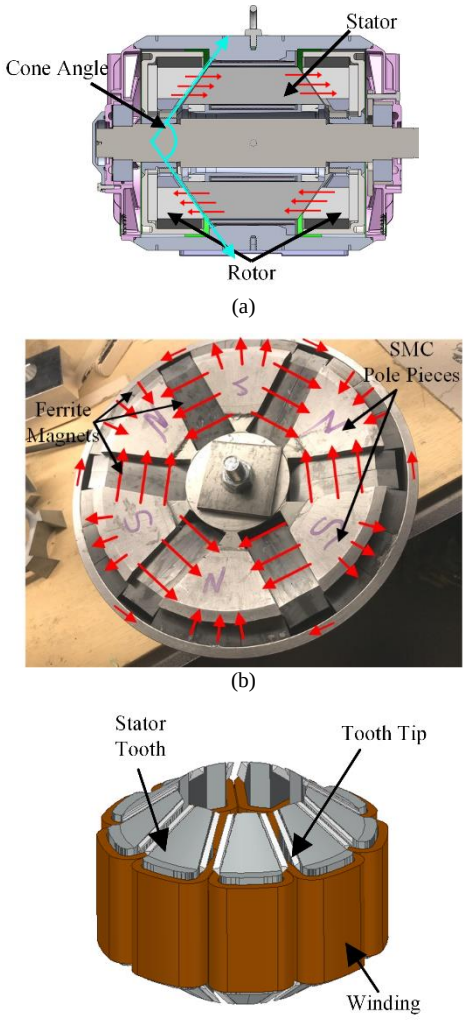

Fig. 1. (a) A transverse-section of the motor, (b) the prototype's rotor, and (c) the magnetically active portions of the stator. Red arrows show the direction of magnetic flux.

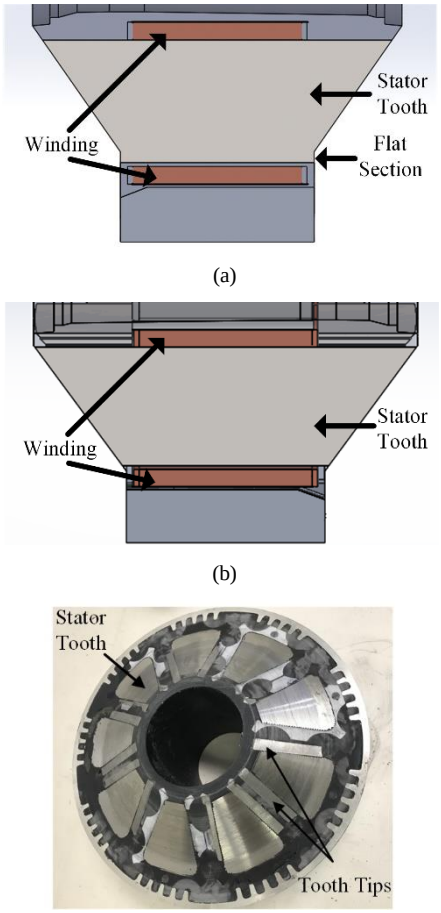

Fig. 2. Transverse sections of (a) a stator design with the flat section and (b) the previous stator design without the flat section and (c) the prototype's stator.

A. *Winding Configuration*

Winding configurations with different wire gauges and different numbers of radial layers were evaluated. Using larger wires increases the cross-sectional area of the windings, which reduces the cross-sectional area of the stator teeth, and increases the axial length of the windings, which increases the axial length of the teeth. Using more radial layers increases the windings' cross-sectional area and reduces the axial length of the windings and stator teeth. The rotor SMC poles were adjusted to maintain the same inner and outer diameters as the stator teeth for each winding configuration. The ratio of the PM surface area adjacent to the SMC poles to the surface area of the SMC poles adjacent to the air gap was kept constant. Table II describes the different winding configurations evaluated, and Fig. 3 illustrates the

TABLE II. WINDING CONFIGURATION

Wire Size (AWG)	Layers	Copper Mass (kg)	Stator Tooth Cross-Sectional Area (mm2)	Stator Tooth Length (mm)	Stator Tooth Mass (kg)
17	7	4.00	1350	63	0.841
17	6	4.14	1552	72	1.098
16.5	6	4.60	1484	76	1.084
17	5	4.23	1758	84	1.437
16	5	5.19	1634	93	1.412
15	5	6.23	1526	101	1.421

torques and efficiencies achieved by each winding configuration. Each configuration has either 294 or 295 turns around each stator tooth.

Increasing the flux through the stator teeth increases the torque; thus, for the same current, designs with larger stator tooth cross-sectional areas achieve higher torques, as shown in Fig. 3(a). However, increasing the stator tooth mass increases the stator core losses. Thus, Fig. 3(b) shows that the 17 AWG 7 layer design, which has the lowest stator tooth mass, achieves the highest efficiency at light loads. However, its low torque per amp coefficient leads to worse efficiencies at heavier loads. Increasing the wire size (lowering the AWG number) reduces the winding resistance, which increases efficiency at heavier loads, where the copper losses dominate the other losses. However, this also increases the mass and cost of the motor and reduces the torque per amp coefficient (due to the reduced stator tooth cross-sectional area). Thus, the 17 AWG 7 layer design was selected to maximize efficiency at lighter loads, such as the 5 kW targeted by the program [1], and minimize motor mass and cost. However, the design is nonetheless capable of producing much larger torques with an efficiency still exceeding 96%, as shown in Fig. 3(b).

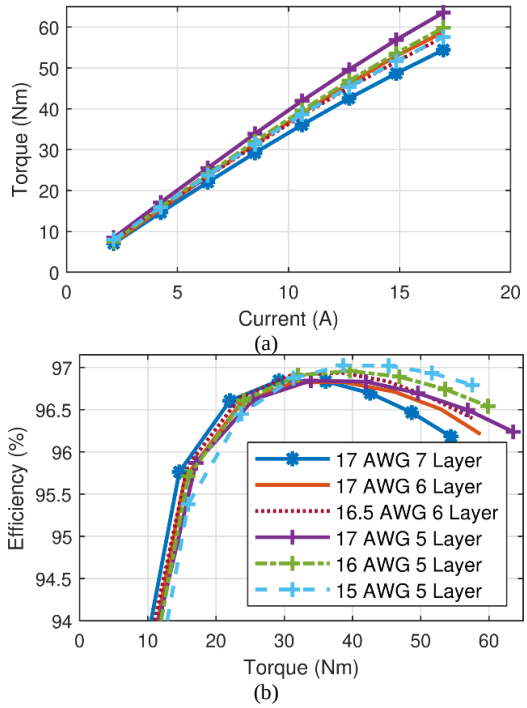

Fig. 3. Variation of (a) torque with current and (b) efficiency with torque for different winding configurations operating at 1800 RPM

B. *Cone Angle*

This topology also introduces cone angle, which is labeled in Fig. 1(a), as a design parameter. The motor investigated in [15], and the designs evaluated in the previous section, have cone angles of 110 degrees; for this section, cone angles of 110, 130, and 150 degrees were evaluated for the winding configuration with 7 radial layers of AWG 17 wire. The torques and efficiencies achieved with these three cone angles are illustrated in Fig. 4.

Increasing the cone angle beyond 110 degrees brings the motor closer to a purely axial air gap; this reduces both the air gap area and the mass of the stator teeth. The reduced air gap area reduces the flux in the stator, which slightly reduces the torque per amp coefficient, as shown in Fig. 4(a). Thus, increasing the cone angle increases the copper losses for a given torque. Accordingly, at heavier loads where the copper losses become dominant, the 150 cone angle designs do not achieve higher efficiencies than the lower cone angle design at heavy loads. However, at light loads, the core losses dominate the copper losses, so the larger cone angle designs, which have less stator mass and, thus, lower core losses, achieve higher efficiencies than the 110 degree design.

C. *Tooth Tips*

Additionally, SMC tooth tips can be added to the stator teeth to help collect more rotor flux and to reduce the magnitude

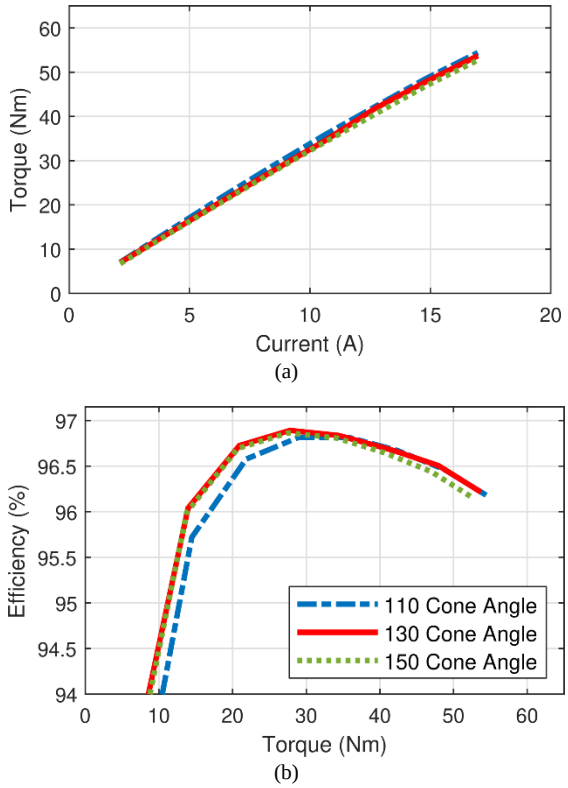

Fig. 4. Variation of (a) torque with current and (b) efficiency with torque for designs with different cone angles operating at 1800 RPM. Each design has 7 layers of 17 AWG wire.

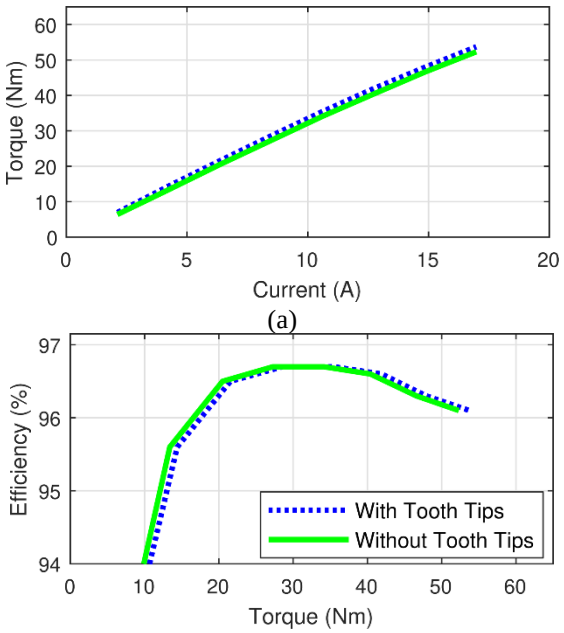

Fig. 5. Variation of (a) torque with current and (b) efficiency with torque for designs with and without SMC tooth tips operating at 1800 RPM. Each design has 7 layers of 17 AWG wire and a 130 degree cone angle.

of the slotting harmonics. Each of the designs in the previous sections employs tooth tips parallel to the air gap surface area. The circumferential width of each tooth tip is 5 mm, the axial height of each tooth tip is 5 mm, and the θ-z cross-section of each tooth tip is an isosceles right triangle. The tooth tips are illustrated in Figs. 1(c) and 2(c). Fig. 5 illustrates the torques and efficiencies achieved by the design with 7 radial layers of AWG 17 wire and a 130 degree cone angle both with and without SMC tooth tips.

As shown in Fig. 5(a), the tooth tips increase the torque slightly by collecting more flux from the rotor. The tooth tips also reduce the core losses on the rotor by reducing the slotting harmonics, but these core losses are already small [15]. There are some small core losses induced in the tooth tips, which can slightly reduce efficiency at light load; however, at heavier loads for a specific torque, the difference in copper losses resulting from the tooth tips can be noticeable.

IV. Efficiency Map

Based on the simulation results from the winding configuration, different cone angle, and tooth tips, the design with 7 layers of 17 AWG wire, a 130 degree cone angle, with stator tooth tips was selected for prototyping. Figs. 6(a) and (b) show its simulated efficiency map, and what percentage of the simulated losses are stator copper losses at each operating point, respectively for total airgap length of 3 mm.

Fig. 6(a) shows that the motor should be able to achieve at least 96% efficiency over a large portion of its operating range. At light loads, the core losses are dominant, so the efficiency increases almost linearly with torque. However, at low speeds and heavy loads, the copper losses become excessive and

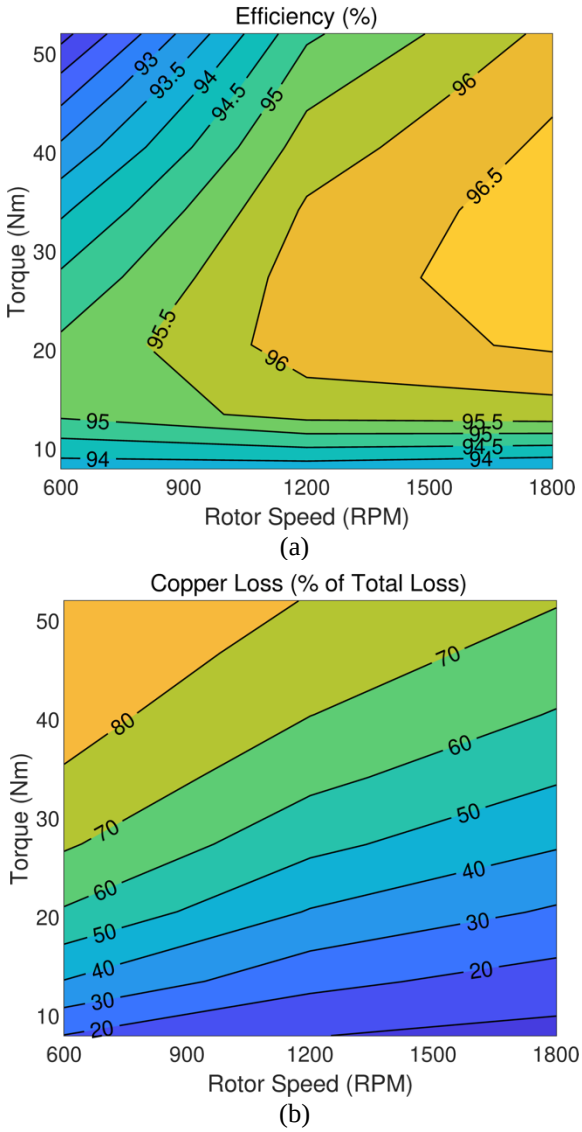

Fig. 6.: Variation of (a) efficiency and (b) copper losses as a percentage of total losses with torque and speed for a design with 7 layers of 17 AWG wire, a 130 degree

reduce the efficiency. Fig. 6(b) shows that at the 1800 RPM, 26Nm (5 kW) design point, there is a balance between the copper losses and the load independent losses (friction and most of the core losses).

Fig. 7 provides the RMS back-emf value at different speed and total airgap lengths. These back-emf results were compared against the measured back-emf used to determine the actual air gap of the prototype motor.

V. Experimental Results

Fig. 8 shows the motor testing setup similar to the testing setup of [15] in which the motor is driven by a Yaskawa A1000 drive and the electrical input power of the motor is measured by a PZ4000 Yokogawa power analyzer. The initial experimental results achieve 96.7% efficiency at 1800 RPM and 26 Nm load

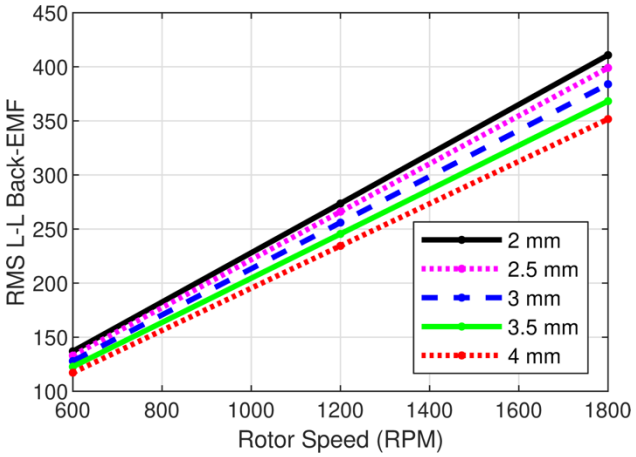

Fig. 7 RMS line to line back EMF at different airgap length

torque. Fig. 9 shows the experimental results over a range of torques and speeds while the efficiency of the previous design is shown as the baseline.

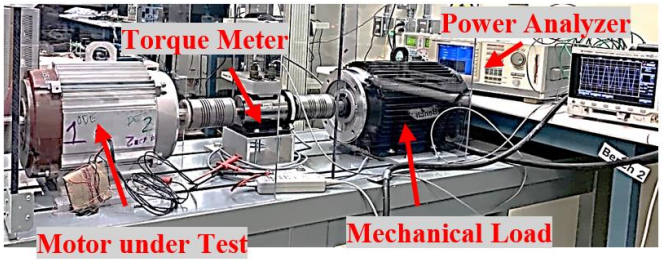

Fig. 8. Experimental test setup

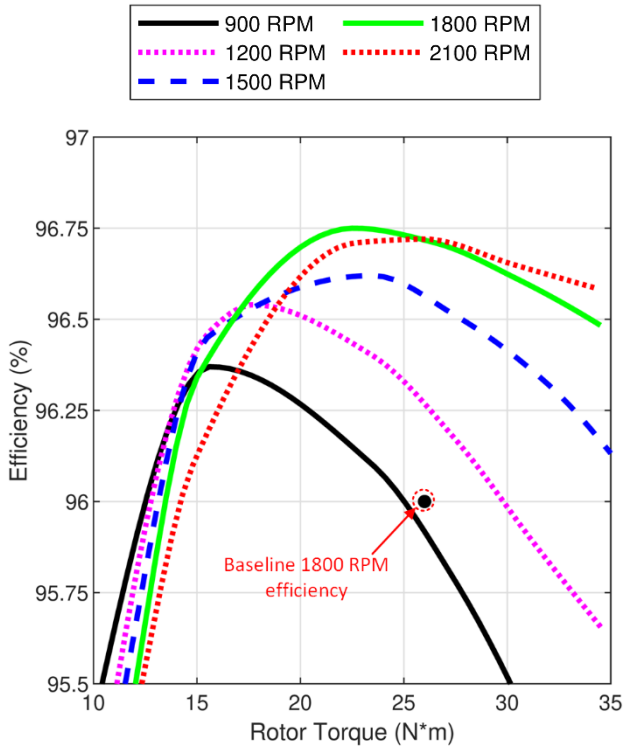

Fig. 9. Efficiency versus torque measured at various speeds

Fig. 10 shows the measured back-emf after the motor was raised to thermal steady-state by running at full load for a few hours. Based on a comparison with Fig. 7, it was determined that the total air gap of the prototype was about 4.2 mm. With the re-evaluated airgap length, the FEA model was simulated at different stator currents and rotor speeds. The results in Fig. 11 show a similar trend of peak efficiency at rated torque except at 2100 RPM. Also, there is a difference at the light loads with a comparison of Figs. 9 and 11. This may be due to an imprecise measurement in experimental testing or underestimating the frequency-related losses in FEA simulations.

Fig. 12 shows the FEA power factor (PF) of the motor at 1800 RPM rotor speed at different torque for maximum torque per amp (MTPA) operation. As a permanent magnet motor, the power factor is relatively high.

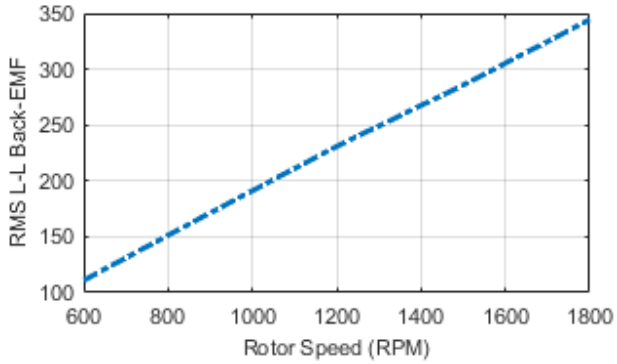

Fig. 10. Line to line Back Emf measured at various speeds

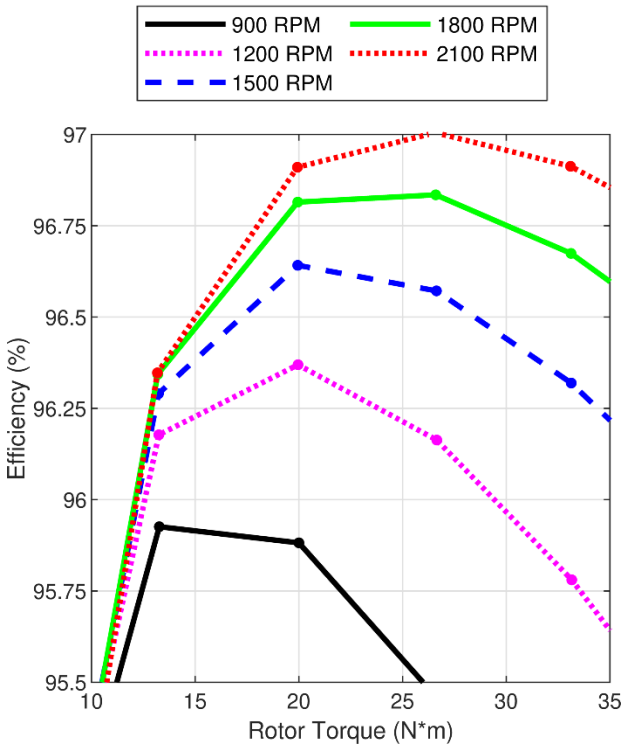

Fig. 11. FEA effieincy vs torque for various speed of actual airgap length

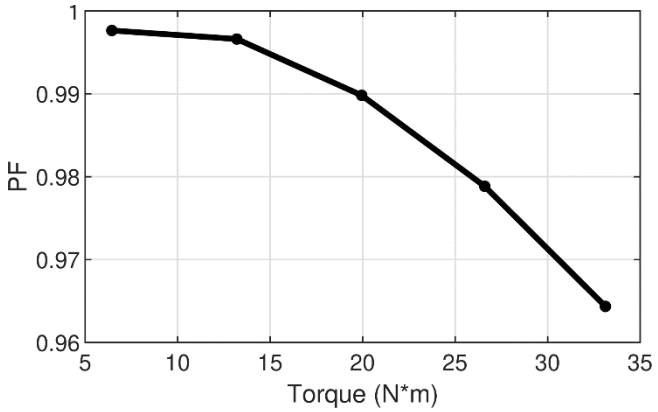

Fig. 12. FEA powerfactor at 1800 RPM at different torque

VI. Conclusions and Future Work

The simulations presented in this paper show that this dual-rotor, single-stator, conical air gap PM motor can achieve much higher efficiencies than similarly sized NEMA frame motors without requiring rare-earth magnets. The impacts of different winding configurations, SMC tooth tips, and cone angle variations were evaluated. A motor with 7 radial layers of 17 AWG wire, a 130 degree cone angle with tooth tips was prototyped and tested. The experimental results show a promising efficiency around 96.7% at the nominal 1800 RPM, 5 kW operating point. Additionally, the prototype's efficiency exceeds 96% over a wide range of torques and speeds.

Acknowledgment

This material was based on the work supported by Department of Energy under Award Number DE-EE0007875. This report was prepared as an account work sponsored by an agency in United States Government. Neither the United States Government nor any agency thereof, nor any their employees, makes any warranty, express or implied, or assumes any legal liability or responsibility for the accuracy, completeness, or usefulness of any information, apparatus, product, or process disclosed, or represents its use would not infringe privately owned rights. Reference herein to any specific commercial product, process, or service by trade name, trademark, manufacturer, or otherwise does not necessarily constitute or imply its endorsement, recommendation, or favoring by the United States Government or any agency thereof. The views and opinions of authors expressed herein do not necessarily state or reflect those of the United States Government or any agency thereof.

Portions of this research were conducted with the advanced computing resources provided by Texas A&M High Performance Research Computing. The authors would like to thank ANSYS for their support of the EMPE lab through the provision of FEA software.

References

[1] "DE-FOA-0001467: Next Generation Electric Machines: Enabling Advanced Technologies," Office of Energy Efficiency and Renewable Energy (EERE), Mar. 9, 2016.

[2] A. T. de Almeida, F. J. T. E. Ferreira, and G. Baoming, "Beyond Induction Motors-Technology Trends to Move Up Efficiency," *IEEE Trans. Ind. Appl*., vol. 50, no. 3, pp. 2103-2114, May/Jun. 2014.

[3] M. J. Melfi, S. Evon, and R. McElveen, "Permanent Magnet Motors for Power Density and Energy Savings in Industrial Applications," in *Proc. Annu. Pulp Paper Ind. Tech. Conf*., 2008, pp. 218-225

[4] E. Sayed, P. Azer, M. Kordic, J. Reimers, B. Bilgin, M. H. Bakr, and A. Emadi, "Design of a Switched Reluctance Motor for a Pump Jack Application," in *Proc. IEEE Elect. Power Energy Conf*., 2018, pp. 1-6.

[5] M. Villani, M. Santececca, and F. Parasiliti, "High-Efficiency Line-Start Synchronous Reluctance Motor for Fan and Pump Applications," in *Proc. IEEE Int. Conf. Elect*. Mach., 2018, pp. 2178-2184.

[6] H. Karkkainen, L. Aarniovuori, M. Niemela, J. Pyrhonen, and J. Kolehmainen, "Technology Comparison of Induction Motor and Synchronous Reluctance Motor," in *Proc. Annu. Conf. IEEE Ind. Electron. Soc*., 2017, pp. 2207-2212.

[7] Regal Beloit, "Marathon Motors Catalog," 2018. Accessed: Jan. 14, 2014. [Online]. Available: https://www.regalbeloit.com/media/Files/Literature/Industries/Marathon_Century_Catalog_Form_MB0030E.pdf.

[8] R. Vartanian, "Permanent Magnet Assisted Synchronous Reluctance Machine (PMa-SynRM) Design and Performance Analysis for Fan and Pump Applications," Ph.D. Dissertation, Dept. Elect. Eng., Texas A&M University, College Station, Texas, USA, 2014.

[9] Y. Tang, and J. A. Kline, "Modeling and Design Optimization of Switched Reluctance Machine by Boundary Element Analysis and Simulation," *IEEE Trans. Energy Convers*., vol. 11, no. 4, pp. 673-680.

[10] J. Ma, J. Li, H. Fang, Z. Li, Z. Liang, L. Xiao, and R. Qu, "Optimal Design of an Axial-Flux Switched Reluctance Motor with Grain-Oriented Electrical Steel," *IEEE Trans. Ind. Appl*., vol. 52, no. 6, pp. 5327-5337, Nov./Dec. 2017.

[11] Y. Sugawara and K. Akatsu, "Characteristics of a Switched Reluctance Motor using Grain-Oriented Electric Steel Sheet," in *Proc. IEEE Int. Conf. Elect. Mach. Sys.*, 2013, pp. 18-23.

[12] R. Pei, L. Zeng, S. Li, and T. Coombs, "Studies on grain-oriented silicon steel used in traction motors," in *Proc. IEEE Int. Conf. Elect. Mach. Sys*., 2017, pp. 1-4.

[13] S. Taghavi and P. Pillay, "A Novel Grain-Oriented Lamination Rotor Core Assembly for a Synchronous Reluctance Traction Motor with a Reduced Torque Ripple Algorithm," *IEEE Trans. Ind. Appl*., vol. 52, no. 5, pp. 3729-3738, Sep./Oct. 2016.

[14] D. Kowal, P. Sergeant, L. Dupre, and A. Van den Bossche, "Comparison of Nonoriented and Grain-Oriented material in an Axial Flux Permanent-Magnet Machine," *IEEE Trans. Magn*., vol. 46, no. 2, pp. 279-285, Feb. 2010.

[15] M. C. Gardner, Y. Zhang, D. Talebi, H. A. Toliyat, A. Crapo, P. Knauer, and H. Willis, "Loss Breakdown of a Dual Conical Rotor Permanent Magnet Motor using Grain Oriented Electrical Steel and Soft Magnetic Composites," in *Proc. IEEE Int. Elect. Mach. and Drives Conf*., 2019, pp. 1067-1074.

[16] "Simulation Versus Experimental Verification [Society News]," *IEEE Ind. Appl. Magazine*, vol. 28, no. 3, pp. 88-94, May-Jun. 2022.

[17] D. Talebi, M. C. Gardner, S. V. Sankarraman, A. Daniar and H. A. Toliyat, "Electromagnetic Design Characterization of a Dual Rotor Axial Flux Motor for Electric Aircraft," in *Proc. IEEE Int. Elect. Mach. and Drives Conf*., 2021, pp. 1-8.

[18] D. Talebi, M. C. Gardner, S. V. Sankarraman, A. Daniar, and H. A. Toliyat, "Electromagnetic Design Characterization of a Dual Rotor Axial Flux Motor for Electric Aircraft," *IEEE Trans. Ind. Appl*, July. 2022.

[19] C. Wiley, D. Talebi, S. V. Sankarraman, M. C. Gardner, and M. Benedict, "Design of a Carbon Fiber Rotor in a Dual Rotor Axial Flux Motor for Electric Aircraft", in *Proc. IEEE Energy Convers. Congr. Expo.*, 2022.

[20] N. Malone et al,. "Investigation of Mass Saving Potential of Zeolite Integrated Motor Thermal Management Systems in All-Electric Commercial Aircraft", in Proc. *Int. Mech. Eng. Congr. and Expo*., 2022.